

Nodeless superconductivity in $4H_b$ -TaS₂ with broken time reversal symmetry

Yuwei Zhou,¹ Fanyu Meng,^{2,3} Yanen Huang,¹ Jiawen Zhang,¹ Jin Zhan,¹ Ye Chen,¹ Yu Liu,¹ Hechang Lei,^{2,3} Michael Smidman,^{1,*} and Huiqiu Yuan^{1,4,5,6,†}

¹*Center for Correlated Matter and School of Physics, Zhejiang University, Hangzhou 310058, China*

²*School of Physics and Beijing Key Laboratory of Opto-electronic Functional Materials & Micro-nano Devices, Renmin University of China, Beijing 100872, China*

³*Key Laboratory of Quantum State Construction and Manipulation (Ministry of Education), Renmin University of China, Beijing 100872, China*

⁴*Institute for Advanced Study in Physics, Zhejiang University, Hangzhou 310058, China*

⁵*Institute of Fundamental and Transdisciplinary Research, Zhejiang University, Hangzhou 310058, China*

⁶*State Key Laboratory of Silicon and Advanced Semiconductor Materials, Zhejiang University, Hangzhou 310058, China*

(Dated: July 28, 2025)

The transition metal dichalcogenide $4H_b$ -TaS₂ exhibits characteristics of topological edge modes and two-component superconductivity with time-reversal symmetry breaking (TRSB). The nature of the superconducting order parameter is a crucial issue that requires experimental investigation. Here, we report measurements of the magnetic penetration depth using a tunnel-diode-oscillator based technique, as well as the specific heat. Both the specific heat and the change in magnetic penetration depth ($\Delta\lambda(T)$) display an exponentially-activated temperature dependence, providing evidence for nodeless superconductivity in $4H_b$ -TaS₂. Moreover, the deduced superfluid density can be well described by a two-gap s -wave model, and such multigap superconductivity is consistent with there being multiple bands crossing the Fermi energy. These results constrain the possible pairing symmetries of $4H_b$ -TaS₂.

PACS number(s):

I. INTRODUCTION

Time-reversal symmetry breaking (TRSB) in superconductors is manifested by the appearance of spontaneous magnetic fields in the superconducting state. Such an additional symmetry breaking at T_c generally requires a degenerate instability channel, leading to a multi-component order parameter, often with nodal superconducting gaps. These order parameters correspond to an unconventional superconducting state [1, 2], as observed in some strongly correlated electronic systems [3–8]. More recently, evidence for superconductivity with TRSB was observed in some weakly correlated materials, such as LaNiC₂ [9], LaNiGa₂ [10, 11], Lu_{5-x}Rh₆Sn_{18+x} [12, 13], CaPtAs [14, 15] and several Re-based superconductors [16–18]. Thus, whether superconductivity with TRSB necessarily originates from an unconventional pairing mechanism or can be realized through conventional electron-phonon pairing requires further investigation in more candidate materials.

The quasi-two-dimensional transition metal dichalcogenide materials exhibit intricate interplay between charge, lattice, and orbital degrees of freedom, giving rise to unusual properties, such as charge density wave phases, superconductivity and topological phases [19–22]. Depending on the stacking arrangement and the unit cell size, diverse structural phases, including $1T$, $2H$, $3R$, $4H_b$, and $6R$, are obtained [23]. The natural van der Waals heterostructure $4H_b$ -TaS₂, consisting of alternating layers of octahedral $1H$ -TaS₂ and trigonal prismatic $1T$ -TaS₂, undergoes a superconducting transition at 2.9 K. $1H$ -TaS₂ exhibits superconductivity at

0.8 K in its bulk form [19], whereas Mott physics plays a crucial role in both bulk and single-layer $1T$ -TaS₂ [24–27]. A chiral superconducting state has been proposed for $4H_b$ -TaS₂ based on muon spin relaxation (μ SR) measurements showing TRSB below the superconducting transition temperature [28]. Moreover, $4H_b$ -TaS₂ has been proposed as a candidate for topological superconductivity based on scanning tunneling spectroscopy measurements, which exhibit signatures of edge modes and zero-bias states in vortex cores [29]. Little-Parks effect measurements reveal π -shifts in the superconducting transition-temperature oscillations, providing possible evidence for a multi-component order parameter [30].

The superconducting gap structure of $4H_b$ -TaS₂ still remains unclear. Theoretically, some symmetry-imposed nodal structures, such as those of the B_{1u} and E_{2g} order parameters, have been suggested [31]. Experimentally, scanning tunneling microscopy (STM) measurements reveal a U-shaped superconducting gap but with a finite in-gap density of states [29]. Moreover, a small residual linear term in zero field and an S-shaped field dependence are observed in thermal conductivity measurements [32], and it was suggested that some Fermi surfaces are fully gapped while others remain gapless. Recent measurements of transverse-field (TF) μ SR evidence fully gapped superconductivity, while the specific heat coefficient exhibits a finite intercept in the $T \rightarrow 0$ limit, which is suggested to be an intrinsic feature in $4H_b$ -TaS₂ [28]. To better understand the superconducting order parameter of $4H_b$ -TaS₂, experiments sensitive to low-energy electronic excitations within the superconducting state are required.

In this article, we probe the gap symmetry of $4H_b$ -

TaS_{1.99}Se_{0.01} single crystals via measurements of the magnetic penetration depth change $\Delta\lambda(T)$ using a tunnel-diode oscillator (TDO) based technique, as well as the specific heat. The $\Delta\lambda(T)$ flattens at low temperatures and shows an exponentially activated behavior, which rules out the presence of nodes, demonstrating fully-gapped superconductivity. Furthermore, the deduced superfluid density and electronic specific heat data can be well fitted by a two-gap *s*-wave model. These results provide evidence for nodeless multigap superconductivity in $4H_b$ -TaS₂.

II. EXPERIMENTAL DETAILS

Single crystals of $4H_b$ -TaS_{1.99}Se_{0.01} were synthesized using the chemical vapor transport method, with 1% Se doping to enhance the stability of the crystal structure, reduce the superconducting transition width, and significantly increase the superconducting volume fraction, as reported in previous studies [28–30, 33–35]. The electrical resistivity $\rho(T)$ and heat capacity $C(T)$ were measured using a Physical Property Measurement System (PPMS) down to 2 K and 0.4 K, respectively. Resistivity measurements were performed on sample (#2) which was also measured using the TDO technique. Four platinum wires were attached to the sample surface using silver paint. The sample mass for the specific heat measurement was 11.8 mg. The magnetization measurements down to 1.8 K were performed using a Magnetic Property Measurement System (MPMS). The temperature dependence of the magnetic penetration depth shift, $\Delta\lambda(T) = \lambda(T) - \lambda(0)$, was measured using a TDO-based technique in a ³He cryostat down to 0.33 K, operating at approximately 7 MHz with a noise level as low as 0.15 Hz [36, 37]. $\Delta\lambda(T)$ can be obtained from the TDO frequency shift $\Delta f(T)$ through $\Delta\lambda(T) = G\Delta f(T)$, where G is the calibration factor determined from the geometry of the coil and the sample [38, 39]. Three samples were oriented using an x-ray Laue, cut into regular shapes, and then separately mounted onto a sapphire rod, which was positioned without direct contact with the coil. The dimensions of the three samples are $725 \times 580 \times 50 \mu\text{m}^3$ (#1), $704 \times 525 \times 60 \mu\text{m}^3$ (#2) and $562 \times 225 \times 495 \mu\text{m}^3$ (#3). One of the samples (#3) was studied with the field perpendicular to the *c* axis, while the others (#1 and #2) were studied with the applied field along the *c* axis. The coil that generates the ac field produces approximately 2 μT , which is much smaller than the lower critical field H_{c1} , thus ensuring that the sample remains in the Meissner state.

III. RESULTS

The temperature dependence of the *ab* plane resistivity $\rho_{ab}(T)$ of a $4H_b$ -TaS_{1.99}Se_{0.01} single crystal from 300 K down to 2 K is displayed in Fig. 1(a). The $\rho_{ab}(T)$ ex-

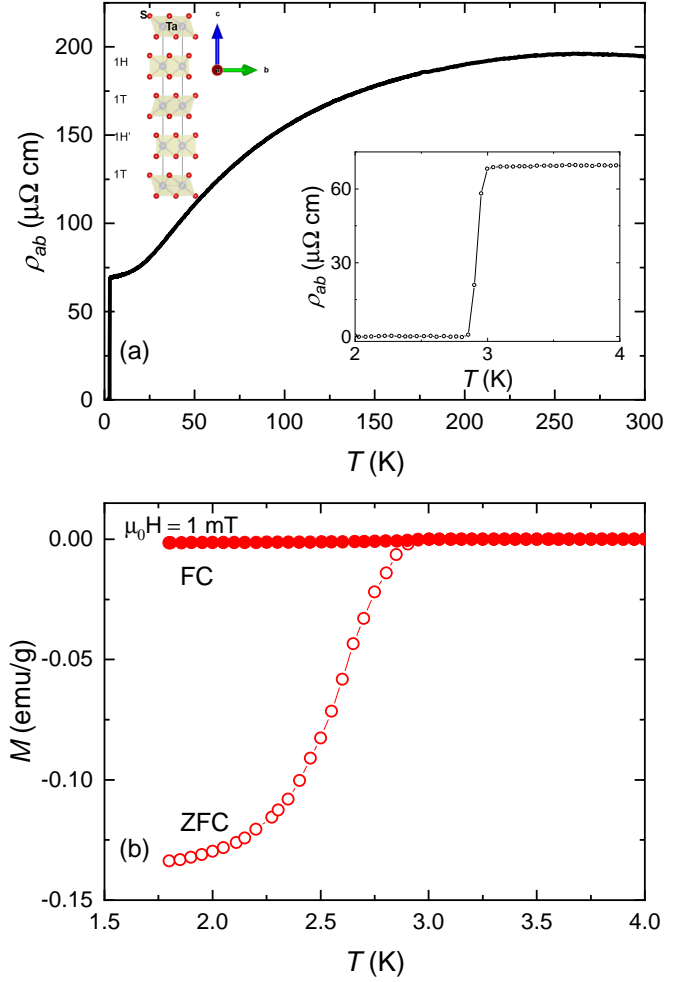


FIG. 1. (Color online) (a) Temperature dependence of the in-plane electrical resistivity $\rho_{ab}(T)$ of $4H_b$ -TaS_{1.99}Se_{0.01} from room temperature down to 2 K. The top-left and bottom-right insets show the crystal structure and the $\rho_{ab}(T)$ near the superconducting transition, respectively. (b) The temperature dependence of magnetization under both zero-field cooling (ZFC) and field-cooling (FC) processes, with a 10 Oe field applied within the *ab* plane.

hibits metallic behavior with a residual normal state resistivity ρ_0 of about $69.3 \mu\Omega \text{ cm}$. The inset shows $\rho_{ab}(T)$ at low temperatures, revealing a clear superconducting transition with an onset at $T_c^{\text{onset}} = 2.96 \text{ K}$ and zero resistivity at $T_c^{\text{zero}} = 2.85 \text{ K}$, consistent with previous results [33]. The temperature dependence of the magnetization is shown in Fig. 1(b) under zero-field and field-cooling processes in an applied magnetic field of 10 Oe. A clear superconducting transition is observed with an onset at around 2.96 K. Using the values of $\gamma_n = 6.228 \text{ mJ mol}^{-1} \text{ K}^{-2}$ from the specific-heat and the $B_{c2}(0) = 1.1 \text{ T}$ [33], the penetration depth at zero temperature $\lambda(0)$ is estimated to be 465 nm using $\lambda(0) = \sqrt{\Phi_0 B_{c2}(0) / \sqrt{24\gamma_n \Delta(0)}}$ [40], consistent with the experimental value $\lambda(0) = 487 \text{ nm}$ derived from μSR [28]. Further combined with $\rho_0 = 69.3 \mu\Omega \text{ cm}$, the mean free path ℓ is estimated to be $\ell = 74.5 \text{ nm}$ [41]. The BCS coherence

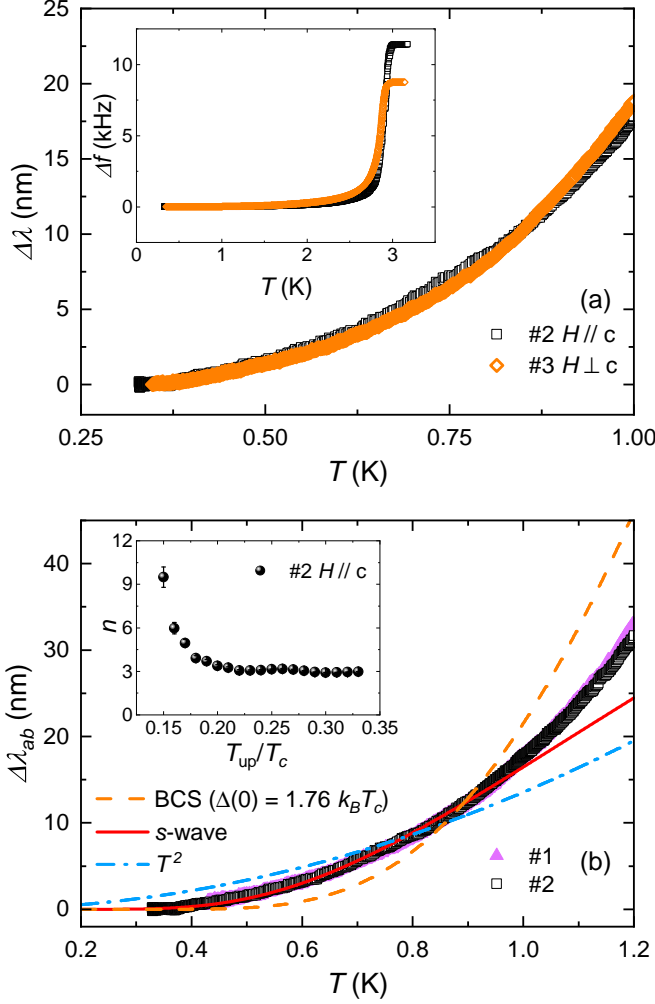


FIG. 2. (Color online) (a) Temperature dependence of the magnetic penetration depth shift $\Delta\lambda(T)$ of $4H_b$ -TaS_{1.99}Se_{0.01} for applied fields along and perpendicular to the c axis. The inset shows the corresponding $\Delta f(T)$ in the temperature range 3.2 K to 0.33 K. (b) $\Delta\lambda_{ab}(T)$ at low temperatures, measured for two samples with fields along the c axis. The solid, dashed-dotted, and dashed lines represent fitting to an s -wave model, quadratic dependence $\sim T^2$, and the weak coupling BCS model, respectively. The exponent n obtained from a power law fit over different temperature ranges, from the lowest measured temperature up to a temperature T_{up} , is shown in the inset.

length ξ_{BCS} can be calculated using $\xi_{GL} = 0.74\xi_{BCS}$, where the Ginzburg-Landau (GL) coherence length is given by $\xi_{GL} = \sqrt{\Phi/2\pi B_{c2}(0)} = 17.26$ nm, which yields $\xi_{BCS} = 23.3$ nm. It can be seen that the mean free path is larger than ξ_{BCS} , indicating that the sample is in the clean limit.

The temperature dependence of the frequency shift, $\Delta f(T)$, from 3.2 K down to 0.33 K with the applied field both along and perpendicular to the c axis are shown in the inset of Fig. 2(a), where a distinct reduction upon cooling around $T_c = 2.96$ K is observed due to superconductivity, consistent with resistivity, magnetic sus-

ceptibility, and specific heat measurements. The low-temperature $\Delta\lambda(T)$ are displayed in Fig. 2(a), with calibration factors of $G = 13.8$ Å/Hz and 10 Å/Hz for the samples with $H \parallel c$ and $H \perp c$, respectively. $\Delta\lambda(T)$ displays nearly identical behavior in both orientations, suggesting that the superconducting state is unlikely to be strongly anisotropic. For $H \parallel c$, the screening currents flow only in the ab plane, probing the in-plane penetration depth shift $\Delta\lambda_{ab}(T)$ [38, 42]. $\Delta\lambda_{ab}(T)$ is plotted for two samples in the main panel of Fig. 2(b) at low temperatures, and this change is derived from $\Delta f(T)$ using $G = 15.7$ Å/Hz and 13.8 Å/Hz calculated for samples #1 and #2, respectively. It is clear that the two samples consistently deviate markedly from the T -linear and T^2 dependences, which are expected for clean-limit superconductors with line nodes and point nodes, respectively. For an isotropic single-band s -wave superconductor, $\Delta\lambda_{ab}(T)$ at $T \ll T_c$ can be approximated by

$$\Delta\lambda_{ab}(T) = \lambda(0) \sqrt{\frac{\pi\Delta(0)}{2k_B T}} \exp\left(-\frac{\Delta(0)}{k_B T}\right), \quad (1)$$

where $\Delta(0)$ is the superconducting gap magnitude at zero temperature. As shown by the solid red line, the experimental data below $T_c/3$ are well described by this model with $\Delta(0) = 0.99(2)k_B T_c$, while it shows a clear deviation from a model with the gap size of $\Delta(0) = 1.76k_B T_c$ derived from weak-coupling BCS theory. The exponential behavior is further supported by fitting the data to a power law, $\Delta\lambda_{ab}(T) \sim T^n$, where the exponent n , obtained from fitting from the lowest measured temperature up to a temperature T_{up} (inset of Fig. 2(b)), consistently exceeds two and increases as the temperature decreases. The deduced superconducting gap from fitting with Eq. 1 of $0.99k_B T_c$ being smaller than the value for the weak-coupling BCS theory, $1.76k_B T_c$, indicates the presence of multiple gaps and/or gap anisotropy.

To further investigate the gap structure of $4H_b$ -TaS_{1.99}Se_{0.01}, we calculated the superfluid density, $\rho_s(T)$, for samples in the clean limit, using $\rho_s(T) = [\lambda(0)/\lambda(T)]^2$, with $\lambda(0) = 487$ nm obtained from μ SR [28]. The $\rho_s(T)$ derived from μ SR measurements in Ref [28] are also displayed, which are consistent with the TDO-method results. The superfluid density is fitted utilizing various gap functions $\Delta_k(T)$, calculated using

$$\rho_s(T) = 1 + 2 \left\langle \int_{\Delta_k}^{\infty} \frac{E dE}{\sqrt{E^2 - \Delta_k(T)^2}} \frac{\partial f}{\partial E} \right\rangle_{FS}, \quad (2)$$

where $f(E, T) = [1 + \exp(E/k_B T)]^{-1}$ is the Fermi-Dirac distribution and $\langle \dots \rangle_{FS}$ represents an average over the Fermi surface [37]. The gap function Δ_k is defined as $\Delta_k(T) = \Delta(T)g_k$, where $\Delta(T)$ corresponds to the temperature dependence of the gap, approximated as [43]

$$\Delta(T) = \Delta(0) \tanh \left\{ 1.82 [1.018 (T_c/T - 1)]^{0.51} \right\}, \quad (3)$$

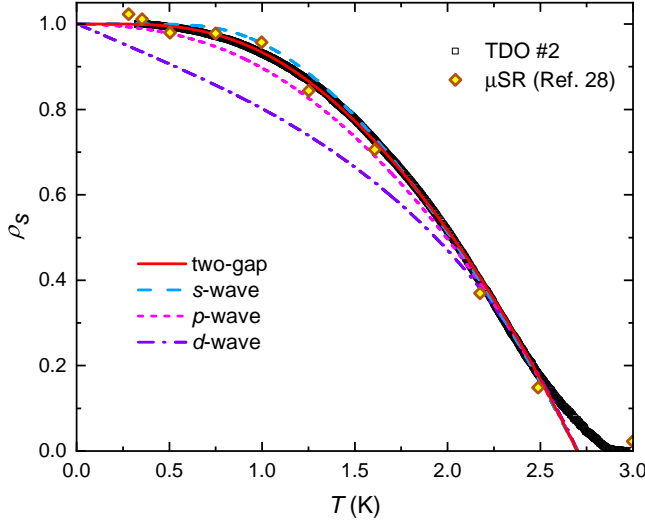


FIG. 3. (Color online) Temperature dependence of the normalized superfluid density $\rho_s(T)$ for sample #2 with $\lambda(0) = 487$ nm. The solid, dashed, short-dashed, and dashed-dotted lines represent the fitting results with two-gap *s*-wave, *s*-wave, *p*-wave, *d*-wave models, respectively. The rhombus symbols show results derived from μ SR measurements from Ref. [28].

and g_k represents the angular dependence of the gap structure. Specifically, $g_k = 1$, $\sin \theta$, and $\cos 2\phi$ correspond to *s*-, *p*-, and *d*-wave superconducting gaps, respectively (θ is the polar angle, and ϕ is the azimuthal angle). The data were fitted up to 2.7 K, as above this temperature, the frequency changes increase sharply, as shown in the inset of Fig. 2(a), which is the onset of the transition to the normal state.

Consistent with the analysis of the magnetic penetration depth, the superfluid density exhibits significant deviations from both the *p*-wave and *d*-wave models (Fig. 3), which have point nodes and line nodes, respectively. A single gap *s*-wave model still does not describe the data well at low temperatures. In contrast, the data across the entire temperature range is fitted well by a two-gap *s*-wave model [43], described by $\rho_s(T) = x\rho_{s1} + (1-x)\rho_{s2}$, where ρ_{s1} and ρ_{s2} are calculated using Eq. 2 for gap magnitudes $\Delta_1(0)$ and $\Delta_2(0)$, respectively, and x is the weight of the contribution from $\Delta_1(0)$. The fitted parameters are $\Delta_1(0) = 0.89(2)k_B T_c$, $\Delta_2(0) = 1.96(1)k_B T_c$ and $x = 0.099(6)$, which corresponds to a weight of the smaller gap of around 10%. The small gap obtained from fitting the superfluid density with a two-gap *s*-wave model is similar to the fitted gap from the analysis of the low-temperature $\Delta\lambda_{ab}$, further corroborating the presence of multiple superconducting gaps.

The total specific heat, plotted as $C(T)/T$, is displayed in the inset of Fig. 4, showing a clear superconducting transition at around $T_c = 2.85$ K, providing evidence for bulk superconductivity. In the normal state, the data were fitted using $C(T)/T = \gamma_n + \beta T^2 + \delta T^4$, where $\gamma_n = 6.228$ mJ mol⁻¹ K⁻², $\beta = 0.386$ mJ mol⁻¹ K⁻⁴, and $\delta = 0.087$ μ J mol⁻¹ K⁻⁶. Here, $C_e = \gamma_n T$ and

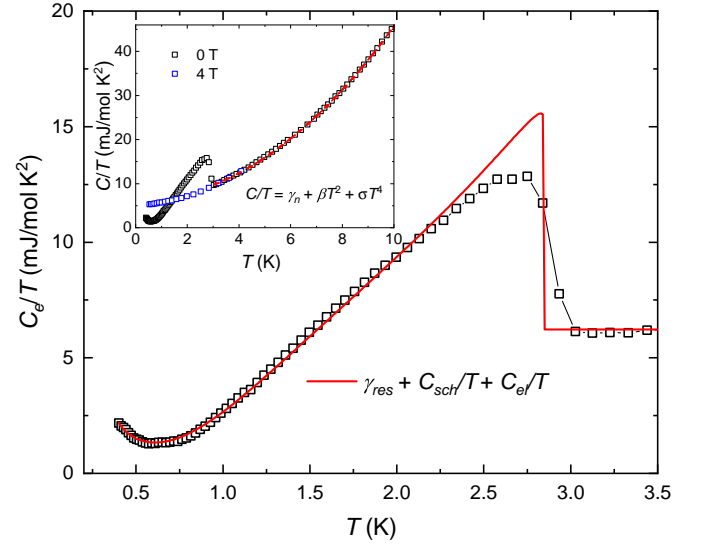


FIG. 4. (Color online) Temperature dependence of the electronic specific heat as C_e/T of $4H_b$ -TaS_{1.99}Se_{0.01}, where the solid line represents the fit with a two-gap *s*-wave model, including a Schottky contribution. The inset shows the total specific heat $C(T)/T$ in zero-field and 4 T, where the dashed line represents the fitting to the normal state contribution.

$C_{ph} = \beta T^3 + \delta T^5$ represent the contributions from normal-state electrons and phonons, respectively, with γ_n being the Sommerfeld coefficient. At low temperatures, $C(T)/T$ shows a noticeable upturn which is suppressed in a high field, likely due to a nuclear Schottky anomaly. After subtracting the phonon contributions, the electronic specific heat $C_e(T)$ of the superconducting state can be described by [44, 45]:

$$C_e(T) = \gamma_{res}T + C_{Schottky}(\Delta E/k_B T) + T dS_{sc}/dT, \quad (4)$$

where γ_{res} represents the residual contribution. The second term is a two-level Schottky anomaly, given by $C_{Schottky}(x) = \frac{nR x^2 e^x}{(1+e^x)^2}$, with ΔE being the level splitting energy, R the gas constant and n the concentration of paramagnetic impurities. The entropy S_{sc} of a single gap superconductor can be calculated by [46]

$$S_{sc} = -\frac{3\gamma_n}{\pi^3} \int_0^{2\pi} \int_0^\infty [f \ln f + (1-f) \ln(1-f)] d\varepsilon d\phi. \quad (5)$$

We analyzed $C_e(T)$ using Eq. 4, where dS_{sc}/dT is calculated using a two gap model, which consists of the sum of single band contributions with gap magnitudes Δ_1 and Δ_2 (Eq. 5), with a relative weight x of the contribution from the former gap. Here we fixed the values of the parameters $\Delta_1(0)$, $\Delta_2(0)$ and x to those from the analysis of the superfluid density, so that the fitted parameters are the two associated with the Schottky term ΔE and n , as well as γ_{res} . As shown by the solid line in Fig. 4, $C_e(T)$ is well fitted throughout the superconducting state, with parameters $\Delta E = 4.6 \times 10^{-24}$ J, $n = 0.00058$, and $\gamma_{res} = 0.3$ mJ mol⁻¹ K⁻². The residual contribution γ_{res} is similar to previous results [28],

which is likely due to a nonsuperconducting fraction, possibly originating from different stacking arrangements of $1T$ and $1H$ layers in $4H_b$ -TaS_{1.99}Se_{0.01}.

IV. DISCUSSION AND CONCLUSIONS

The exponentially-activated behavior of $\Delta\lambda(T)$ at low temperatures evidences nodeless superconductivity in $4H_b$ -TaS_{1.99}Se_{0.01}, consistent with previous studies of the specific heat and μ SR [28]. Moreover, our analysis of $\Delta\lambda(T)$ and the derived superfluid support the presence of multigap superconductivity, whereby the gap magnitude from the analysis of $\Delta\lambda(T)$ at low temperatures is considerably less than the weak coupling BCS value, and is also much smaller than that from fitting the superfluid density to a model with a single isotropic gap. Furthermore this one-gap model cannot well describe the superfluid density over the full temperature range. In contrast, the superfluid density is well fitted by a two-gap s -wave model, and the smaller gap from this fitting is close to the value from the low temperature analysis of $\Delta\lambda(T)$, providing clear evidence for multigap superconductivity. Moreover, the same parameters deduced from fitting the two-gap model to the superfluid density, can also consistently describe the specific heat.

The conclusion of multigap superconductivity is consistent with presence of multiple bands crossing the Fermi energy, as revealed by angle-resolved photoemission spectroscopy (ARPES) measurements and electronic structure calculations [35]. Besides the inner pocket along the $K - M - K'$ line, which originates from the $1H$ layer, ARPES also observes several shallow pockets around the Γ point in the normal state, which originate from the $1T$ layers but are notably different from the bulk bands of $1T$ -TaS₂. This is further supported by STM results, which identify depleted flat bands with a weak density of states crossing the Fermi level [47]. These different bands

may play an important role in the superconductivity and are likely associated with superconducting gaps of different sizes.

Based on the analysis of the irreducible representations (irreps) of the hexagonal point group and the pronounced two-dimensional nature of $4H_b$ -TaS_{1.99}Se_{0.01}, only four irreps need to be considered: the trivial irrep A_{1g} , B_{1u} , and the two-dimensional irreps E_{2g} and E_{1u} [30, 31]. Our results demonstrate that the superconducting gap structure of $4H_b$ -TaS_{1.99}Se_{0.01} is nodeless, ruling out the B_{1u} and E_{2g} order parameters, as both exhibit symmetry enforced nodes in the gap function. Considering the TRSB inferred from μ SR measurements [28], complex $p + ip$ states are favored over the even-parity A_{1g} representation, but this identification requires further verification via phase-sensitive experiments.

In summary, we have investigated the superconducting pairing symmetry of $4H_b$ -TaS_{1.99}Se_{0.01} single crystals using magnetic penetration depth measurements and the specific heat. The penetration depth data below $T_c/3$ show a clear exponentially activated temperature dependence, indicating a nodeless superconducting gap. The temperature dependence of the superfluid density and specific heat can be well described by nodeless two-gap superconductivity, which is consistent with the presence of multiple Fermi surfaces originating from both the $1H$ and $1T$ layers in $4H_b$ -TaS_{1.99}Se_{0.01}.

ACKNOWLEDGMENTS

This work was supported by the National Key R&D Program of China (Grant No. 2022YFA1402200, No. 2023YFA1406303, No. 2022YFA1403800 and 2023YFA1406500), the National Natural Science Foundation of China (Grants No. 12034017, No. 12494592, No. 12222410, No. 12274459 and No. 12174332)

* Corresponding author: msmidman@zju.edu.cn

† Corresponding author: hgyuan@zju.edu.cn

- [1] M. Sigrist and K. Ueda, Phenomenological theory of unconventional superconductivity, *Reviews of Modern physics* **63**, 239 (1991).
- [2] S. K. Ghosh, M. Smidman, T. Shang, J. F. Annett, A. D. Hillier, J. Quintanilla, and H. Yuan, Recent progress on superconductors with time-reversal symmetry breaking, *Journal of Physics: Condensed Matter* **33**, 033001 (2020).
- [3] G. Luke, A. Keren, L. Le, W. Wu, Y. Uemura, D. Bonn, L. Taillefer, and J. Garrett, Muon spin relaxation in UPT₃, *Physical review letters* **71**, 1466 (1993).
- [4] G. M. Luke, Y. Fudamoto, K. Kojima, M. Larkin, J. Merrin, B. Nachumi, Y. Uemura, Y. Maeno, Z. Mao, Y. Mori, *et al.*, Time-reversal symmetry-breaking superconductivity in Sr₂RuO₄, *Nature* **394**, 558 (1998).
- [5] J. Xia, Y. Maeno, P. T. Beyersdorf, M. Fejer, and A. Kapitulnik, High resolution polar kerr effect measurements

of Sr₂RuO₄: Evidence for broken time-reversal symmetry in the superconducting state, *Physical review letters* **97**, 167002 (2006).

- [6] R. Heffner, J. Smith, J. Willis, P. Birrer, C. Baines, F. Gygax, B. Hitti, E. Lippelt, H. Ott, A. Schenck, *et al.*, New phase diagram for (U,Th)Be₁₃: A muon-spin-resonance and H_{c1} study, *Physical review letters* **65**, 2816 (1990).
- [7] E. Schemm, R. Baumbach, P. Tobash, F. Ronning, E. Bauer, and A. Kapitulnik, Evidence for broken time-reversal symmetry in the superconducting phase of URu₂Si₂, *Physical Review B* **91**, 140506 (2015).
- [8] E. Schemm, W. Gannon, C. Wishne, W. Halperin, and A. Kapitulnik, Observation of broken time-reversal symmetry in the heavy-fermion superconductor UPT₃, *Science* **345**, 190 (2014).
- [9] A. D. Hillier, J. Quintanilla, and R. Cywinski, Evidence for time-reversal symmetry breaking in the noncen-

- trosymmetric superconductor LaNiC_2 , Physical review letters **102**, 117007 (2009).
- [10] A. D. Hillier, J. Quintanilla, B. Mazidian, J. F. Annett, and R. Cywinski, Nonunitary triplet pairing in the centrosymmetric superconductor LaNiGa_2 , Physical Review Letters **109**, 097001 (2012).
 - [11] Z. Weng, J. Zhang, M. Smidman, T. Shang, J. Quintanilla, J. F. Annett, M. Nicklas, G. Pang, L. Jiao, W. Jiang, *et al.*, Two-gap superconductivity in LaNiGa_2 with nonunitary triplet pairing and even parity gap symmetry, Physical Review Letters **117**, 027001 (2016).
 - [12] A. Bhattacharyya, D. Adroja, J. Quintanilla, A. Hillier, N. Kase, A. Strydom, and J. Akimitsu, Broken time-reversal symmetry probed by muon spin relaxation in the caged type superconductor $\text{Lu}_5\text{Rh}_6\text{Sn}_{18}$, Physical Review B **91**, 060503 (2015).
 - [13] A. Wang, Z. Nie, F. Du, G. Pang, N. Kase, J. Akimitsu, Y. Chen, M. Gutmann, D. Adroja, R. Perry, *et al.*, Nodeless superconductivity in $\text{Lu}_{5-x}\text{Rh}_6\text{Sn}_{18+x}$ with broken time reversal symmetry, Physical Review B **103**, 024503 (2021).
 - [14] W. Xie, P. Zhang, B. Shen, W. Jiang, G. Pang, T. Shang, C. Cao, M. Smidman, and H. Yuan, CaPtAs : A new non-centrosymmetric superconductor, Science China Physics, Mechanics & Astronomy **63**, 237412 (2020).
 - [15] T. Shang, M. Smidman, A. Wang, L.-J. Chang, C. Baines, M.-K. Lee, Z. Nie, G. Pang, W. Xie, W. Jiang, *et al.*, Simultaneous nodal superconductivity and time-reversal symmetry breaking in the noncentrosymmetric superconductor CaPtAs , Physical review letters **124**, 207001 (2020).
 - [16] D. Singh, J. Barker, A. Thamizhavel, D. M. Paul, A. Hillier, and R. Singh, Time-reversal symmetry breaking in the noncentrosymmetric superconductor Re_6Hf : Further evidence for unconventional behavior in the α -Mn family of materials, Physical Review B **96**, 180501 (2017).
 - [17] G. Pang, Z. Nie, A. Wang, D. Singh, W. Xie, W. Jiang, Y. Chen, R. Singh, M. Smidman, and H. Yuan, Fully gapped superconductivity in single crystals of noncentrosymmetric Re_6Zr with broken time-reversal symmetry, Physical Review B **97**, 224506 (2018).
 - [18] D. Singh, S. KP, J. Barker, D. M. Paul, A. Hillier, and R. Singh, Time-reversal symmetry breaking in the non-centrosymmetric superconductor Re_6Ti , Physical Review B **97**, 100505 (2018).
 - [19] J. A. Wilson, F. Di Salvo, and S. Mahajan, Charge-density waves and superlattices in the metallic layered transition metal dichalcogenides, Advances in Physics **24**, 117 (1975).
 - [20] J. Wilson, F. Di Salvo, and S. Mahajan, Charge-density waves in metallic, layered, transition-metal dichalcogenides, Physical review letters **32**, 882 (1974).
 - [21] S. Manzeli, D. Ovchinnikov, D. Pasquier, O. V. Yazyev, and A. Kis, 2D transition metal dichalcogenides, Nature Reviews Materials **2**, 1 (2017).
 - [22] Y. Liu, L. Li, W. Lu, R. Ang, X. Liu, and Y. Sun, Coexistence of superconductivity and commensurate charge density wave in $4\text{Hb-TaS}_{2-x}\text{Se}_x$ single crystals, Journal of Applied Physics **115** (2014).
 - [23] F. Di Salvo, B. Bagley, J. Voorhoeve, and J. Waszczak, Preparation and properties of a new polytype of tantalum disulfide (4Hb-TaS_2), Journal of Physics and Chemistry of Solids **34**, 1357 (1973).
 - [24] Y. Fei, Z. Wu, W. Zhang, and Y. Yin, Understanding the mott insulating state in 1T-TaS_2 and 1T-TaSe_2 , AAPPS Bulletin **32**, 20 (2022).
 - [25] K. T. Law and P. A. Lee, 1T-TaS_2 as a quantum spin liquid, Proceedings of the National Academy of Sciences **114**, 6996 (2017).
 - [26] H. Lin, W. Huang, K. Zhao, S. Qiao, Z. Liu, J. Wu, X. Chen, and S.-H. Ji, Scanning tunneling spectroscopic study of monolayer 1T-TaS_2 and 1T-TaSe_2 , Nano Research **13**, 133 (2020).
 - [27] B. Sipos, A. F. Kusmartseva, A. Akrap, H. Berger, L. Forró, and E. Tutiš, From mott state to superconductivity in 1T-TaS_2 , Nature Materials **7**, 960 (2008).
 - [28] A. Ribak, R. M. Skiff, M. Mograbi, P. Rout, M. Fischer, J. Ruhman, K. Chashka, Y. Dagan, and A. Kanigel, Chiral superconductivity in the alternate stacking compound 4Hb-TaS_2 , Science advances **6**, eaax9480 (2020).
 - [29] A. K. Nayak, A. Steinbok, Y. Roet, J. Koo, G. Margalit, I. Feldman, A. Almoalem, A. Kanigel, G. A. Fiete, B. Yan, *et al.*, Evidence of topological boundary modes with topological nodal-point superconductivity, Nature physics **17**, 1413 (2021).
 - [30] A. Almoalem, I. Feldman, I. Mangel, M. Shlafman, Y. E. Yaish, M. H. Fischer, M. Moshe, J. Ruhman, and A. Kanigel, The observation of π -shifts in the little-parks effect in 4Hb-TaS_2 , Nature Communications **15**, 4623 (2024).
 - [31] M. H. Fischer and J. Goryo, Symmetry and gap classification of non-symmorphic SrPtAs , Journal of the Physical Society of Japan **84**, 054705 (2015).
 - [32] H. Wang, Y. Jiao, F. Meng, X. Zhang, D. Dai, C. Tu, C. Zhao, L. Xin, S. Huang, H. Lei, *et al.*, Evidence for multiband gapless superconductivity in the topological superconductor candidate 4Hb-TaS_2 , arXiv preprint arXiv:2412.08450 (2024).
 - [33] F. Meng, Y. Fu, S. Pan, S. Tian, S. Yan, Z. Li, S. Wang, J. Zhang, and H. Lei, Extreme orbital ab-plane upper critical fields far beyond the pauli limit in $4\text{Hb-Ta}(\text{S},\text{Se})_2$ bulk crystals, Physical Review B **109**, 134510 (2024).
 - [34] E. Persky, A. V. Bjørlig, I. Feldman, A. Almoalem, E. Altman, E. Berg, I. Kimchi, J. Ruhman, A. Kanigel, and B. Kalisky, Magnetic memory and spontaneous vortices in a van der waals superconductor, Nature **607**, 692 (2022).
 - [35] A. Almoalem, R. Gofman, Y. Nitzav, I. Mangel, I. Feldman, J. Koo, F. Mazzola, J. Fujii, I. Vobornik, J. Sanchez Barriga, *et al.*, Charge transfer and spin-valley locking in 4Hb-TaS_2 , npj Quantum Materials **9**, 36 (2024).
 - [36] C. T. Van Degrift, Tunnel diode oscillator for 0.001 ppm measurements at low temperatures, Review of Scientific Instruments **46**, 599 (1975).
 - [37] R. Prozorov and R. W. Giannetta, Magnetic penetration depth in unconventional superconductors, Superconductor Science and Technology **19**, R41 (2006).
 - [38] R. Prozorov, R. Giannetta, A. Carrington, and F. Araujo-Moreira, Meissner-london state in superconductors of rectangular cross section in a perpendicular magnetic field, Physical Review B **62**, 115 (2000).
 - [39] R. Prozorov and V. G. Kogan, Effective demagnetizing factors of diamagnetic samples of various shapes, Physical review applied **10**, 014030 (2018).
 - [40] F. Gross, B. Chandrasekhar, D. Einzel, K. Andres, P. Hirschfeld, H. Ott, J. Beuers, Z. Fisk, and J. Smith, Anomalous temperature dependence of the magnetic field

- penetration depth in superconducting UBe_{13} , *Zeitschrift für Physik B Condensed Matter* **64**, 175 (1986).
- [41] T. Orlando, E. McNiff Jr, S. Foner, and M. Beasley, Critical fields, Pauli paramagnetic limiting, and material parameters of Nb_3Sn and V_3Si , *Physical Review B* **19**, 4545 (1979).
 - [42] J. Fletcher, A. Carrington, P. Diener, P. Rodiere, J.-P. Brison, R. Prozorov, T. Olheiser, and R. Giannetta, Penetration depth study of superconducting gap structure of 2H-NbSe_2 , *Physical review letters* **98**, 057003 (2007).
 - [43] A. Carrington and F. Manzano, Magnetic penetration depth of MgB_2 , *Physica C: Superconductivity* **385**, 205 (2003).
 - [44] Y. Wang, T. Plackowski, and A. Junod, Specific heat in the superconducting and normal state (2-300 K, 0-16 T), and magnetic susceptibility of the 38 K superconductor MgB_2 : evidence for a multicomponent gap, *Physica C: Superconductivity* **355**, 179 (2001).
 - [45] H. Yang, J.-Y. Lin, H. Li, F. Hsu, C.-J. Liu, S.-C. Li, R.-C. Yu, and C.-Q. Jin, Order parameter of MgB_2 : a fully gapped superconductor, *Physical review letters* **87**, 167003 (2001).
 - [46] F. Bouquet, Y. Wang, R. Fisher, D. Hinks, J. Jorgensen, A. Junod, and N. Phillips, Phenomenological two-gap model for the specific heat of MgB_2 , *Europhysics Letters* **56**, 856 (2001).
 - [47] A. Kumar Nayak, A. Steinbok, Y. Roet, J. Koo, I. Feldman, A. Almoalem, A. Kanigel, B. Yan, A. Rosch, N. Avraham, *et al.*, First-order quantum phase transition in the hybrid metal–mott insulator transition metal dichalcogenide 4Hb-TaS_2 , *Proceedings of the National Academy of Sciences* **120**, e2304274120 (2023).
 - [48] Yuwei Zhou. "Nodeless superconductivity in 4Hb-TaS_2 with broken time reversal symmetry" [Data set], 2025. doi:10.5281/zenodo.15688310.